Probing the impact of energetic argon ions on the structural properties of ZnO:Al/TiO$_2$ heterostructures

C. P. Saini, A. Barman, N. Kumar, R. Cours, S. Joulie, V. Serin, A. Claverie, A. K. Sinha, D. Kanjilal, and A. Kanjilal

---

Articles you may be interested in

The effect of Ti^{+} ion implantation on the anatase-rutile phase transformation and resistive switching properties of TiO$_2$ thin films
Journal of Applied Physics **124**, 155303 (2018); 10.1063/1.5045550

Oxygen mediated phase transformation in room temperature grown TiO$_2$ thin films with enhanced photocatalytic activity
Applied Physics Letters **113**, 084103 (2018); 10.1063/1.5040916

Analysis of the optical parameters of amorphous ternary oxides Sn$_{1-x}$Zn$_x$O and Sn$_{1-x}$Ni$_x$O processed by combinatorial ion-beam sputter deposition
Journal of Applied Physics **124**, 155701 (2018); 10.1063/1.5046898

Tuning hydrogen adsorption on pure and doped ZnO (000$\bar{1}$) surfaces by a simple electron counting model
Journal of Applied Physics **124**, 155302 (2018); 10.1063/1.5050544

A theoretical and experimental formalism of electronic structure of BFO:Cr thin films and modulation of their electrical properties upon visible light illumination
Journal of Applied Physics **124**, 155304 (2018); 10.1063/1.5038841

Pressure induced structural phase transition in rare earth sesquioxide Tm$_2$O$_3$: Experiment and ab initio calculations
Journal of Applied Physics **124**, 155901 (2018); 10.1063/1.5049223

Probing the impact of energetic argon ions on the structural properties of ZnO:Al/TiO₂ heterostructures

C. P. Saini,[1,2] A. Barman,[2] N. Kumar,[1] R. Cours,[3] S. Joulie,[3] V. Serin,[3] A. Claverie,[3] A. K. Sinha,[4] D. Kanjilal,[1] and A. Kanjilal[2,a)]

[1]*Inter-University Accelerator Centre, Aruna Asaf Ali Marg, New Delhi 110 067, India*
[2]*Department of Physics, School of Natural Sciences, Shiv Nadar University, NH-91, Tehsil Dadri, Gautam Buddha Nagar, Uttar Pradesh 201 314, India*
[3]*CEMES-CNRS and Université de Toulouse, 29 rue J. Marvig, 31055 Toulouse, France*
[4]*Indus Synchrotron Utilization Division, Raja Ramanna Center for Advanced Technology, Rajendra Nagar, Indore, Madhya Pradesh 452013, India*

The efficacy of 50 keV Ar⁺-ion irradiation toward the interfacial and stoichiometric engineering of strained Al-doped ZnO (AZO)/TiO₂ heterostructure is systematically investigated using a variety of experimental techniques, notably by cross-sectional transmission electron microscopy. Glancing-angle X-ray diffraction evidences the release of in-plane compressive stress from the as-grown AZO/TiO₂ bilayer structure at a critical fluence of 1×10^{16} ions/cm², and we discuss in the light of micro-cracks and voids formation combined with the dewetting phenomenon. Ion irradiation also leads to an improvement of stoichiometry in both top AZO and underneath amorphous TiO₂ layers, as manifested by depth-dependent energy dispersive X-ray spectroscopy owing to the large diffusion of oxygen toward the AZO/TiO₂ interfacial region through the AZO defect sites. Such ion beam induced self-healing in stoichiometry of AZO/TiO₂ heterostructure has been attributed to a conjunction of sputtering and diffusion phenomena involving the constituent elements (Zn, Ti, and O). Further increase in ion fluence up to 5×10^{16} ions/cm² causes a complete deterioration of the heterostructure with the formation of a graded layer via intermixing of these elements, followed by the evolution of voids. *Published by AIP Publishing.* https://doi.org/10.1063/1.5045762

I. INTRODUCTION

Low-energy ion bombardment (LEIB) is a remarkable and versatile technique for structural modification of thin films owing to controlled generation of surface defects, especially via interstitials and vacancies.[1,2] LEIB is, in fact, ubiquitous in the present industrial technology due to its control over impurity in a predetermined depth and density by appropriate choice of ion beam energy and fluence (i.e., ions/cm²).[3,4] Among various metal oxides, LEIB is intensively used in transition-metal oxides not only for understanding the defect propagation, especially oxygen vacancies but also for exploring their structural modulation/evolution.[5] As titanium oxide (TiO₂) and Al-doped ZnO (AZO) are the key model systems for many practical and theoretical studies[6,7] and also play a prominent role as anti-reflective coating (ARC) and transparent conductive oxide (TCO) layers, especially for optoelectronic and next generation solar cells,[8,9] they are attractive targets for ion beam driven structural modifications. In fact, their higher stability and tolerance to non-stoichiometry allow an extensive exploration of morphologies and physical properties. For instance, structural modification through the development of nano-ripples and nanostructures on AZO surfaces by irradiating with energetic ions and their consequences in physical properties have been reported.[10,11] Besides self-organized nano-channel assisted

resistive switching,[12,13] we also demonstrated the efficacy of Ar⁺-ions in realizing TiO₂-based optical and hydrophobic properties by structural modification in the presence of oxygen vacancies.[14,15] Moreover, Pabon *et al.* exhibited a clear transformation of TiO₂ into a single crystalline TiO film by low energetic Ar⁺-ion irradiation.[16] Above studies on metal oxides clearly indicate that both structure and stoichiometry play a dominant role to dictate their physical properties and so for tuning. Moreover, the growth of an AZO film on a thin TiO₂ layer leads to a bilayer heterostructure, possessing an attractive feature in the field of photocatalysis,[17] water splitting,[18] and also for enhancing the anti-reflective performance of solar cells,[9] and many more. Despite several studies on ion beam induced structural modification of TiO₂ and AZO considered separately, detailed investigation of ion beam induced modification of bilayer AZO/TiO₂ heterostructures, especially their microstructure, is still lacking. Clearly, the nature of complexity increases in bilayer structure, mainly at interfaces because of the increase in ion beam mediated diffusion and intermixing of constituent elements in each other. Moreover, reports on few highly influential factors in AZO/TiO₂ heterostructure such as interface effect, strain, and chemical state with LEIB are very scarce to the best of our knowledge. This situation is undesirable, as all physical properties depend ultimately on the structure and interfaces involved.

In this article, the efficacy of 50 keV Ar⁺-ions in controlling the structure and composition of AZO/TiO₂ heterostructure on pristine Si will be demonstrated using a combination

a)Electronic mail: aloke.kanjilal@snu.edu.in

of experimental techniques, notably by transmission electron microscopy (TEM). It will be shown that the critical fluence of 1×10^{16} ions/cm^2 leads to the release of the tensile strain that developed initially during the AZO growth on the TiO$_2$ layer, probably through a dewetting mechanism. Moreover, we evidenced a dramatic restoration in stoichiometry of the AZO and underneath amorphous TiO$_2$ layers at the same critical fluence. Moreover, a complete deterioration of the AZO/TiO$_2$ heterostructure at the highest ion fluence of 5×10^{16} ions/cm^2 along with the formation of voids will be shown.

II. EXPERIMENTAL

Initially, pieces of $500\,\mu$m thick p-type Si(100) with 1×1 cm^2 area were cleaved and cleaned ultrasonically by deionized water to remove any undesired contamination from the surface. Following this, wafers were dipped into 10% HF solution for 30 s to remove the native oxide from the surface. In order to fabricate a multilayer structure on such a Si substrate, initially about a 10 nm thick TiO$_2$ layer was grown at room temperature (RT) by RF magnetron sputtering (Excel Instruments) using 100 W power supply. The deposition parameters for the TiO$_2$ layer can be found in detail in Ref. 14. Following this, about 95 nm thick AZO was deposited on to the previously grown TiO$_2$ layer at RT by a separate/dedicated RF sputtering system (Excel Instruments) using 50 W power supply. Highly pure Ar gas (99.999%) was introduced into the chamber with a flow rate of 30 sccm while the working pressure was maintained at 5 mTorr during deposition. The substrate-to-target distance was kept at 8 cm with a substrate rotational speed of 12 rpm to have a uniform film thickness. 6 mm thick 2 in. diameter targets (MTI Corp., purity 99.99%) of AZO and TiO$_2$ were used. The as-grown AZO/TiO$_2$ heterostructures were irradiated at RT by 50 keV Ar$^+$-ions under normal incidence, keeping a beam current of $\sim 1\,\mu$A and fluences in the range of $0.1-5 \times 10^{16}$ ions/cm^2.

The surface morphologies of as-grown AZO/TiO$_2$/Si before and after ion beam bombardment were investigated by field-emission scanning electron microscopy (SEM; Carl Zeiss) and atomic force microscopy (AFM; Park, XE-007). The thicknesses of AZO and TiO$_2$ films were estimated by a stylus surface profilometer with a resolution of 0.5 nm (Bruker, DektakXT), whereas evolution of the strain was measured by glancing-angle X-ray diffraction (GXRD) with 15 keV X-rays (wavelength $\sim$0.0827 nm) at the Angle Dispersive X-ray Diffraction Beamline (BL-12) of the Indus-2 synchrotron radiation facility with a storage ring operated at 2.5 GeV at the Raja Ramanna Centre for Advanced Technology Indore, India. Moreover, ion beam irradiation induced structural evolution along with intermixing of bilayer films was studied by cross-sectional TEM (XTEM) using a Tecnai FEI (Cs corrected), while elemental/compositional variation was examined by energy dispersive X-ray spectroscopy (EDS) using Philips CM20. All TEM specimens were prepared by Focused Ion Beam (FIB Helios dual beam) after depositing a Pt layer on the sample surface to protect the surface.

III. RESULTS

Before ion irradiation, the impact of 50 keV Ar$^+$-ions on the AZO layer was examined by Stopping and Range of Ions in Matter (SRIM 2013) calculations. Here, Fig. 1 shows the atomic distribution of incident (argon ions) and displaced recoil atoms (Zn, Al, and O) as a function of film thickness, extracted for the fluence of 1×10^{16} ions/cm^2. For a better comparison, the atomic distribution of target elements prior to ion irradiation (as-grown sample) is also indicated by dashed lines (blue for Zn, red for Al, and olive for O) assuming uniform across the AZO layer. As discerned, after ion irradiation the atomic concentration of recoil atoms are large to the surface and fall off gradually for larger thicknesses region. The sputtering yield of AZO extracted from full cascade SRIM simulation is found to be $\sim$8.34 atoms/ion. Therefore, sputtered AZO thicknesses, calculated from sputtering yields for the fluence of 1×10^{16} and 5×10^{16} ions/cm^2 are found to be 18 ± 1 nm and 90 ± 5 nm, respectively.
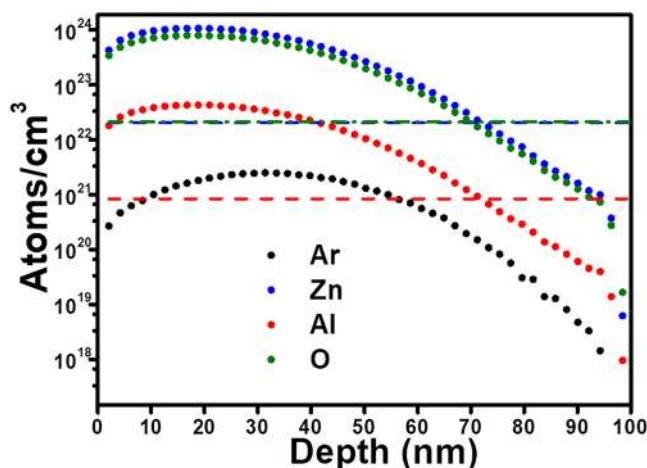

FIG. 1. Thickness dependent atomic variation by incident 50 keV Ar$^+$-ions, showing displaced atoms in the AZO layer by SRIM calculation with a fluence of 1×10^{16} ions/cm^2. The atomic concentration of target elements for the as-grown sample was also shown by dashed straight lines for comparison.
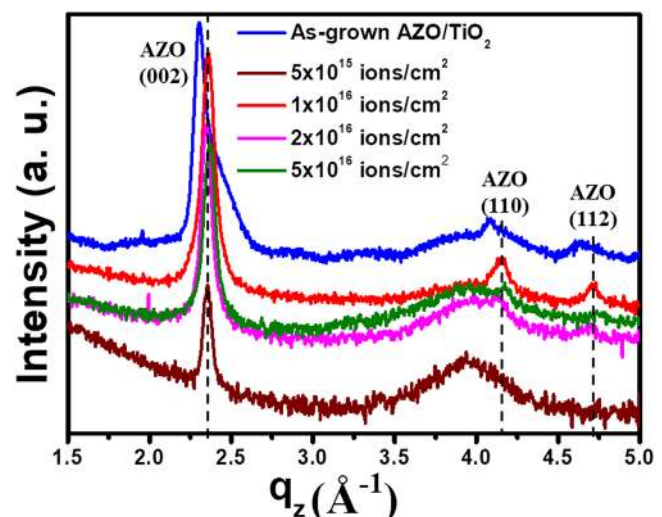

FIG. 2. Typical GXRD patterns of the AZO/TiO$_2$ bilayer structures before and after 50 keV Ar$^+$-ion beam bombardment.

However, sputtered thickness strongly depends upon the local environment created by bombardment of energetic Ar^+-ions as can be seen from Fig. 1, which is not taken into account by static SRIM calculations. It is thus important to note that from the onset of ion irradiation and up fluences approximately of the order of 1×10^{16}, the interface between AZO and TiO_2 is not affected by bombardment while for larger fluences, due to sputtering, this interface and the TiO_2/SiO_2 interface can be affected by ion beam mixing.

To understand the influence of energetic ions on the AZO/TiO_2 bilayer structure, a detailed structural analysis has been carried out by GXRD for an incidence angle of ~0.3°. Typical GXRD patterns of the AZO/TiO_2 bilayer structure before and after ion irradiation are displayed in Fig. 2. Since the data were acquired at 15 keV incident energy by using synchrotron radiation facility rather than the laboratory scale X-rays of energy ~8 keV, Bragg's angle (θ) is converted to momentum vector (q_z) and plotted on x axis of curve by using relation q_z ($Å^{-1}$) = 4πsinθ/λ so that it becomes independent of incident wavelength. Here λ refers to X-ray wavelength and unit is taken in angstrom (Å). As discerned, a most intense peak appeared in the spectra is associated with the reflection from the AZO (002) plane, suggesting the preferential orientation of grains along c-axis. However, close inspection further revealed that ion irradiation leads to shifting of such peak position from lower q_z (~2.30) for the as-grown sample to higher q_z value (~2.36). Moreover, the peaks appearing at q_z = ~4.09 and ~4.64, assigned to the reflections from (110) and (112) planes, respectively, also exhibit a similar trend with ion bombardment. In fact, the significant deviation in q_z value in case of the as-grown AZO layer is suggesting the evolution of a tensile strain which decreases by ion irradiation. This strain probably results from the reaction of the layer to some in-plane compressive stress originating from the AZO/TiO_2 interfacial mismatch.[19,20] In plane compressive stress was calculated on

the basis of a biaxial strain model by using the following relation[19,21] [σ = (2C_{13} − C_{33}(C_{11} + C_{12})/C_{13}) × (c − c_o)/c_o, where C_{11}, C_{12}, C_{13}, and C_{33} are the elastic stiffness constants, respectively, whereas c and c_o correspond to the lattice parameter of hexagonal (wurtzite) cell in the strained and strain-free layers. The generally admitted values of elastic stiffness constants for AZO are[19]: C_{11} = 2.1 × 10^{11} N/m^2, C_{12} = 1.2 × 10^{11} N/m^2, C_{13} = 1.05 × 10^{11} N/m^2, and C_{33} = 2.1 × 10^{11} N/m^2. After putting all coefficient values in the equation, σ becomes −4.5 × 10^{11} (c − c_o)/c_o N/m^2. The calculated values of lattice constant along c axis before and after ion irradiation extracted from the peak position of (002) plane are shown in Fig. S1 (see the supplementary material). Considering an effective area of modification mainly due to elastic collision of a single 50 keV Ar^+ ion of ~1 $Å^2$ (i.e., ~10^{-16} cm^2), the fluence of 1×10^{16} ions/cm^2 covers a total surface area of 1×1 cm^2 without any overlapping of Ar^+-ions. Under this condition, we found that maximum peak shift toward the one for ZnO powder (standard value) occurs for this fluence and thus we have chosen the sample irradiated with a fluence of 1×10^{16} ions as a reference. Therefore, the in-plane compressive residual stress was determined for the as-grown AZO layer with respect to reference (with fluence of 1×10^{16} ions/cm^2) to be −10.2 GPa. Such calculated relative stresses for the fluence of 5×10^{15} and 1×10^{16} ions/cm^2 are also now summarized in Table S1 in the supplementary material along with the absolute value [by taking the c_o (0.2603 nm)[22] for stress free ZnO system]. Close inspection of the (002) peak in the as-grown one further reveals an asymmetricity on the right side of peak, suggesting the distribution of compressive regions with respect to main peak (i.e., some regions are strained and some are not in the as-grown layer). However, irradiation with increasing ion fluence led to a relatively lower FWHM and higher symmetry in the (002) peak as evidenced from Fig. 2, assessing the release of strain consecutively to the ion irradiation. On the other hand, no reflection peak from the underneath TiO_2 layer was found in the spectra, indicating the formation of an amorphous film. Since the data were acquired in GXRD mode where the penetration depth of X-rays is reduced by three orders of magnitude and typically in the range of a few nm,[23] and omega = theta condition is also not satisfied (i.e., diffraction vector is not normal to the sample surface), no characteristics peak from the underneath Si(100) substrate was found in the recorded spectra.

In order to image the change in surface morphology and roughness with increasing ion fluence, detailed AFM investigation was carried out in tapping mode. Typical AFM topography of the as-grown AZO/TiO_2 bilayer structure is shown in Fig. 3(a), showing granular growth of the AZO layer all over the surface. From topography, the calculated average height of AZO grains was found to be in the order of ~4 ± 1 nm. However, 50 keV Ar^+-ion bombardment leads to modifying surface morphology of the AZO films. For example, a gradual evolution of grains, probably resulting from the growth by Ostwald ripening, was noticed up to a fluence of 2×10^{16} ions/cm^2 as exhibited in Figs. 3(b) and 3(c). In fact, a systematic increase in height of the AZO grains from 13 ± 2 to 25 ± 3 nm for 1×10^{16} to 2×10^{16} ions/cm^2,
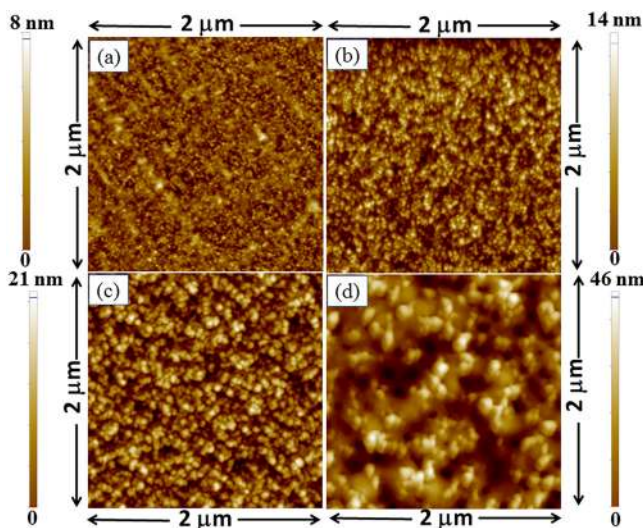

FIG. 3. Typical AFM images of AZO/TiO_2 bilayer on Si surfaces for (a) as-grown, and for 50 keV Ar^+-ion irradiated samples with fluences of (b) 1×10^{16} ions/cm^2, (c) 2×10^{16} ions/cm^2, and (d) 5×10^{16} ions/cm^2. Here the color scale bar represents the height modulation from the sample surface.

respectively, was observed. Further increase in ion fluence up to 5×10^{16} ions/cm^2, however, leads to the sputtering of surface atoms, as evident from Fig. 3(d), causing a significant increment in AZO grains height (~40 nm). Complementary SEM studies have also been conducted for a better understanding.

Typical plan-view SEM image of the as-grown AZO/TiO$_2$ heterostructure is shown in Fig. 4(a), showing a grain-like structure in the AZO layer grown by RF magnetron sputtering. However, an evolution of grains has been recorded under the exposure of 50 keV Ar$^+$-ions. For instance, microcracks were noticed at surfaces when irradiated with a fluence of 1×10^{16} ions/cm^2 followed by the formation of a wrinkle-like pattern at a fluence of 2×10^{16} ions/cm^2 [see Figs. 4(b) and 4(c)]. Further increase in ion fluence up to 5×10^{16} ions/cm^2 leads to the formation of rough surfaces [see Fig. 4(d)] due to sputtering of the surface atoms followed by the formation of small voids in Si in the range of 70-80 nm, consistently with the above mentioned AFM results.

In order to understand the change in surface morphology and structural modification of AZO/TiO$_2$ heterostructure with increasing ion fluence, detailed microstructural investigations have been carried out in some selected samples by XTEM. A typical bright field XTEM image of the as-grown AZO/TiO$_2$/Si sample in Fig. 5(a) shows the formation of smooth and conformal growth of the AZO film on TiO$_2$. The magnified view of the dashed circular region [Fig. 5(a)] further illustrates the crystalline nature of the film with an average thickness of ~95 ± 2 nm [see Fig. 5(b)]. Moreover, close inspection revealed the existence of TiO$_2$ film underneath the AZO layer. High-resolution TEM (HRTEM) image as shown in Fig. 5(c), marked by a dashed circle in Fig. 5(b), however, confirms the amorphous nature of the TiO$_2$ film with an average thickness of ~10 nm, consistent with our profilometer results. In addition,
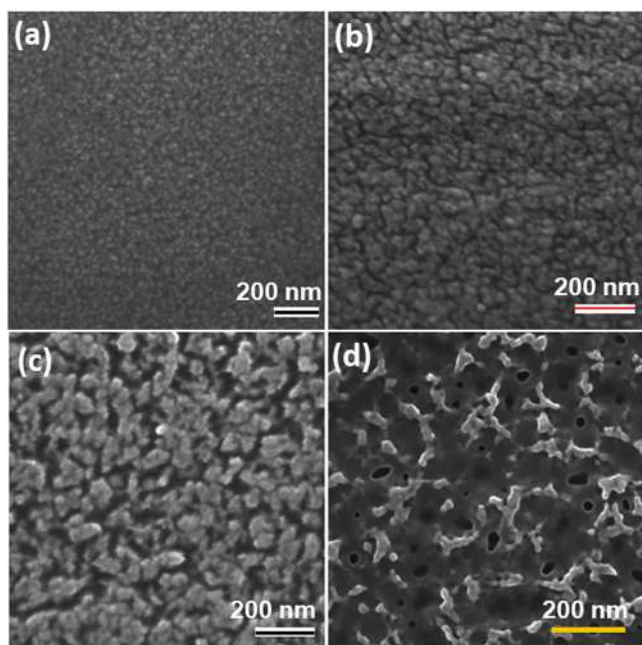

FIG. 4. Plan-view SEM image of the AZO/TiO$_2$ bilayer structure on Si for (a) as-grown, while Ar$^+$ ion irradiated ones are shown for fluences of (b) 1×10^{16}, (c) 2×10^{16}, and (d) 5×10^{16} ions/cm^2, respectively.

careful analysis at the AZO/TiO$_2$ interface also confirmed the formation of an intermediate layer, whereas formation of a very thin (5 ± 1 nm) native oxide (SiO$_2$) layer at the TiO$_2$/Si interface is also visible. The origin of this native oxide layer can be attributed to the diffusion of oxygen radicals during the growth of TiO$_2$ films.[24]

Moreover, the XTEM image of the AZO/TiO$_2$ heterostructure after bombarding with a fluence of 1×10^{16} ions/cm^2 is depicted in Fig. 5(d), revealing a considerable reduction in AZO thickness (~83 ± 2 nm) owing to the sputtering of AZO film. Moreover, owing to continuous Ar$^+$-ion implantation, the density of AZO is likely to be modified and thus affects the sputtering rate. Close inspection further shows an unexpected increment in the underneath TiO$_2$ thickness from 10 ± 1 to 14 ± 1 nm [see Fig. 5(e)].

In order to compare the composition variation before and after ion irradiation, typical EDS traces of the constituent elements, recorded across the bilayer structure before and after ion exposure, are exhibited in Fig. 5(f), while extracted values are summarized in Table I. As can be seen from Table I, the relative Zn concentration in the as-grown sample is significantly higher than that of O, indicating the deviation in stoichiometry of the as-grown AZO film. The reason behind the formation of O deficient AZO film is likely to be the lack of O$_2$ gas incorporation during the growth of the AZO film. On the other hand, ion beam exposure at a fluence of 1×10^{16} ions/cm^2 reduces the AZO thickness [see Fig. 5(f)] as seen on the XTEM images. Since the surface binding energy of Zn (1.35 eV) is smaller than that of O (2 eV), ion beam irradiation helps to restore the regular stoichiometric within the AZO film owing to preferential sputtering of Zn and further diffusion and readjustment of O atoms. Moreover, the evolution in Zn valency with ion irradiation is also modest, as evidenced by RT XANES spectra (see Fig. S2 in the supplementary material). Although XANES is sensitive to the near surface region, EDX and XANES clearly suggest the formation of a stoichiometric and in phase AZO film at a fluence of 1×10^{16} ions/cm^2. Besides this, trapping of Ar$^+$-ions within the AZO film during ion exposure has also been witnessed in the recorded spectra also in good agreement with the SRIM results (see Fig. 1). On the other hand, a considerable increment in the FWHM value of Ti peak with ion exposure was also noticed. Close inspection at the TiO$_2$/AZO interface also confirmed the diffusion of O in the AZO matrix and vice versa which in turn leads to alter the TiO$_2$ stoichiometry. This investigation clearly demonstrates that the ion irradiation with optimum energy and fluence can be used to tune the stoichiometry of the material in the desired way.

Further increase in ion fluence up to 5×10^{16} ions/cm^2 leads to the creation of damage in the AZO/TiO$_2$ matrix followed by the formation of voids [see Fig. 6(a)]. In particular, the HRTEM image within the dashed circle in Fig. 6(a), as shown by Fig. 6(b), shows the formation of bigger voids in the range of 40-50 nm along with small ones. In fact, the appearance of such bigger voids can probably be attributed to the coalescence of smaller ones at a fluence of 5×10^{16} ions/cm^2. Moreover, as discerned from Figs. 6(b) and 6(c), ion bombardment leads to intermixing of the AZO and TiO$_2$
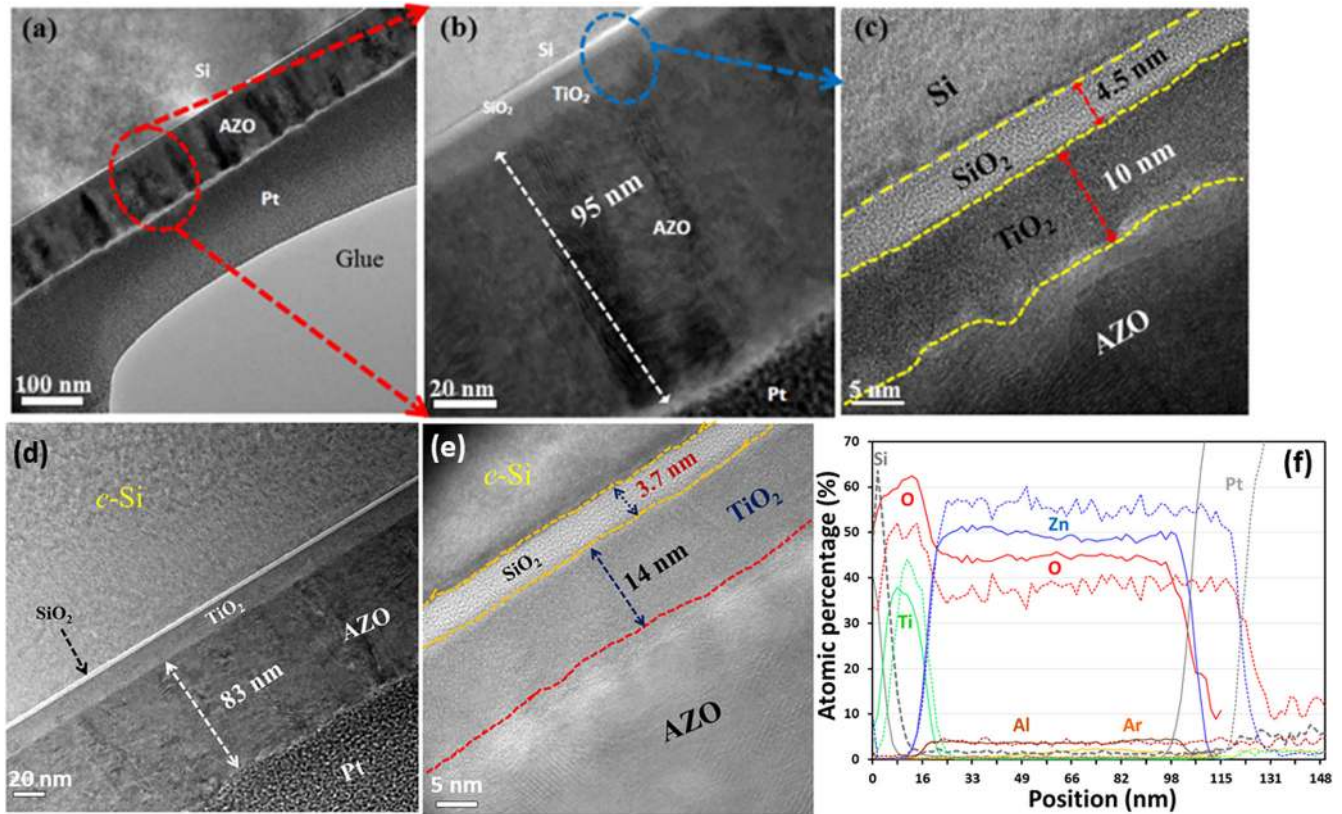
FIG. 5. (a) XTEM image of the as-grown sample; (b) HRTEM image of the red dashed circle region of (a). Whereas (c) represents the HRTEM image from the blue dashed circle in (b), confirming the existence of ∼10 nm thick amorphous TiO$_2$ layer below AZO. A thin (∼4.5 nm thick) native oxide layer is also visible below TiO$_2$. The XTEM and corresponding HRTEM images of 1×10^{16} ions/cm^2 irradiated sample are shown by (d) and (e), respectively. (f) Depth dependent EDS spectra of AZO/TiO$_2$ bilayer before Ar$^+$ ion irradiation (dotted lines) and after irradiation with a fluence of 1×10^{16} ions/cm^2 (solid lines), illustrating the change in thickness and composition due to ion beam sputtering. Here "0" represents the interface region of the Si and TiO$_2$ layers. Here, a thin Pt layer was deposited prior to TEM sample preparation by FIB for protecting the top surface of AZO.

layers via formation of Ti, Zn, and O rich graded layers followed by the reduction in overall film thickness of the combined AZO/TiO$_2$ structure owing to the sputtering of surface atoms. The resultant film thickness is therefore not uniform and varies (from 58 nm to zero) throughout the surface [Figs. 6(b) and 6(c)]. In this scenario, the formation of such giant voids makes the surface rough, and this is also consistent well with AFM results (discussed above). Further inspection of the HRTEM image illustrates the development of an amorphous layer near the surface of the crystalline Si substrate

(c-Si), enriched with O up to a depth of ∼50 nm from the surface. In addition, diffusion of Si into the AZO/TiO$_2$ composite layer was also detected.

IV. DISCUSSION

There are a number of important facts which have been established along this study. As discerned from Figs. 3(a) and 4(a), the as-grown AZO layer is granular in nature. The evolution of these grains can be explained in the light of Volmer-Weber type of nucleation of adatoms on the TiO$_2$ surface.[25] In addition, the as-grown AZO layer exhibits an inhomogeneous in-plane compressive stress (−10.2 GPa) induced by the lattice mismatch between the AZO (c = 5.2057 Å and a = 3.2497 Å)[26] and underneath TiO$_2$ (c = 9.5172 Å a = 3.7862 Å)[27] layers and leads to the formation of strain in the AZO film. Although the AZO layer directly on the Si substrate also exhibits an in-plane compressive stress which is in the range of −4 to −6 GPa,[20,21] in our case, it relatively increased to −10.2 GPa (see Table S1 in the supplementary material) in the presence of the TiO$_2$ layer on the Si substrate (where the calculated values were determined with respect to the film irradiated with a critical fluence of 1×10^{16} ions/cm^2). On the other hand, irradiation with 50 keV Ar$^+$-ions up to a fluence of 1×10^{16} ions/cm^2 led to the development of micro-cracks and voids owing to the formation of wrinkle-like

TABLE I. Variation in the elemental atomic percentage before and after ion irradiation.

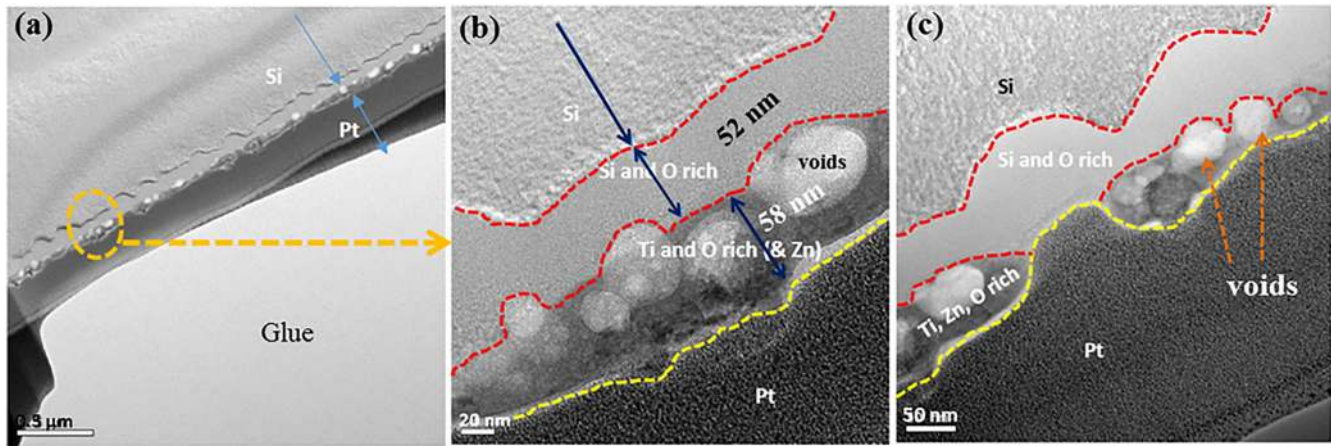|		Atomic percentage (%) ± 1	
Composition	Element	As-grown sample	1×10^{16} ions/cm^2 irradiated sample
For TiO$_2$ layer	Ti	43	36
	O	52	62
	Zn	2	1
	Si	3	1
For AZO layer	Zn	57.5	49
	O	39	45
	Al	3.5	4
	Ar	0	2

FIG. 6. (a) XTEM image of Ar$^+$-ion irradiated AZO/TiO$_2$ bilayer structure at a fluence of 5×10^{16} ions/cm^2 while corresponding HRTEM images are shown in (b) and (c), respectively.

patterns [see Fig. 4(b)] which in turn decreases the relative stress significantly from the top AZO layer. In fact, ion irradiation displaces AZO atoms in the top surface layers, where the O atoms and vacancies both diffuse deep inside the layer and eventually reach the interfacial region (AZO/TiO$_2$). These vacancies agglomerate and create micro-cracks and voids and consequently help to release the in-plane compressive stress. Park *et al.* have also shown the relaxation of tensile strain in ZnO layer grown on Al$_2$O$_3$ substrate by the formation of micro-cracks,[26] generated when the residual stress exceeds the yield strength of either of the film surface or the underlying substrate.[28,29] Moreover, as discerned from Fig. 2, the increasing ion fluence also leads to decrease in FWHM of (002) peak. In fact, by comparing GXRD, TEM, and SEM results, it appears that the decrease in FWHM is mainly associated with the increase in average crystallite size, where the role of dislocation and cracks are mostly concentrated near grain boundaries before terminating in voids. Therefore, the observed decrease in FWHM is dominated by the former one.

Moreover, structural evolution through the development of a wrinkle-like pattern in the AZO/TiO$_2$ heterostructure can be explained in the framework of irradiation induced dewetting process. Actually, the interplay and competition between thermodynamics and kinetics, generally, dictate the dewetting process. Thermodynamics drives a system toward a low surface energy state which is energetically the most favored situation, whereas kinetics prevents the system to go for the low surface energy condition.[30] Since AZO and TiO$_2$ films have been deposited on the Si surface at RT, the atoms cannot move up to significant distances owing to the lack of sufficient kinetic energy, required to overcome the surface energy barrier, and ultimately form a continuous and strained metastable film. However, Ar$^+$-ion bombardment up to a fluence of 2×10^{16} ions/cm^2, as depicted in Fig. 4(c), leads the system toward thermodynamical equilibrium due to the loss of rigid bound between the film and substrate followed by the evolution of micro-cracks in AZO/TiO$_2$ heterostructure for achieving minimum surface free energy.[30]

The stoichiometric restoration of AZO films after irradiation with a fluence of 1×10^{16} ions/cm^2 can be explained by

the modification of Zn and O concentrations [see Fig. 5(f)]. Energetic Ar$^+$-ions lose their energy in the AZO layer due to collisions with the constituent atoms and further displace them from their regular lattice sites either by recoil or sputtering process. This in turn results the creation of interstitials and vacancies. For evaluating this phenomenon, the sputtering yield has been extracted by SRIM calculations, revealing that for Zn it is 5.15 atoms/ion, which is significantly higher than that of O (3.15 atoms/ion) due to the lower surface binding energy of Zn. This consequently leads to a reduction of Zn concentration with ion irradiation. In particular, as Zn is heavier than O, it gets preferably sputtered from the surface during irradiation. On the other hand, the possibility of O self-diffusion through grain boundaries and vacancies/defects induced either by thermal treatment or exposure to oxygen rich atmosphere is higher.[31–34] Therefore, the observed enhancement in O concentration, here, can be attributed to the diffusion of O atoms from ambient through localized dislocations and defects created by the energetic Ar$^+$-ions. Apart from this, the increment in TiO$_2$ thickness likely to be ion beam induced swelling of the TiO$_2$ film owing to the out-diffusion of oxygen atoms from the native oxide layer for reducing the difference in chemical potential at their interfaces. This is also consistent with the observed reduction in native oxide thickness to ~3.7 nm. Such stoichiometric restoration in AZO/TiO$_2$ heterostructure without a deteriorating structure can act as a potential platform for optoelectronic and photovoltaic applications. Here, AZO can be used as a TCO, whereas TiO$_2$ serves as ARC, though electrical performance is also essential for achieving a complete picture which is under investigation now and reported elsewhere.

Further increase in ion fluence (i.e., 5×10^{16} ions/cm^2) leads to the formation of a Ti, Zn, and O rich graded layer due to the intermixing of atoms followed by the evolution of voids in AZO/TiO$_2$ matrix. Although the stopping range of 50 keV Ar$^+$-ions, extracted from SRIM calculations, is lower (~32 nm), after some time and for large enough ion fluence, the AZO thickness is reduced by sputtering to the depth at which mixing of AZO/TiO$_2$ can occur. Moreover, using SRIM simulation, full energy damage cascade plot of 50 keV Ar$^+$-ions (see Fig. S3 in the supplementary material) also

reveals the possibility of some fraction of Ar^{+}-ions to reach the underneath TiO_2 layer and also the Si substrate, and hence can participate in ion beam mixing. Irradiation with such low energy Ar^{+}-ions, in particular, causes a ballistic mixing at the AZO/TiO_2 interface owing to elastic collision cascades[35] and dominated by the recoil atoms.[36] According to time scale range, effects of collisions in material can be divided into two major events: (i) *prompt effects*, occurring in the picosecond range, is dominated by Recoil implantation and cascade mixing process, whereas (ii) *delay effects*, arising in the nanosecond range, is dominated by radiation enhanced diffusion or thermal spike diffusion process.[35] Here, elastic collision causes the significant evolution of point defects in the surface region of AZO which further promote the redistribution of O through diffusion across the AZO/TiO_2 interfaces.

V. CONCLUSIONS

In conclusion, we report the structural and compositional modification in AZO/TiO_2 bilayer structure irradiated by 50 keV Ar^{+}-ions. Although the as-grown AZO layer was oxygen deficient and thus heavily and inhomogeneously strained, ion beam bombardment at a critical fluence of 1×10^{16} ions/cm^2 resulted in the release of this stress through the formation of microcracks due to dewetting of the bilayer structure. Moreover, bombardment at this critical fluence also led to the restoration of the regular stoichiometries of the AZO and TiO_2 films. In particular, for some critical fluence, the large diffusion of O through the ion beam induced AZO defect sites was noticed, while ion beam induced self-healing in stoichiometry of the AZO/TiO_2 heterostructures has also been noted and attributed to an interplay between sputtering and diffusion of the constituent elements (Zn, Ti, and O). Further increase in ion fluence up to 5×10^{16} ions/cm^2 leads to the complete deterioration of the AZO/TiO_2 heterostructure and to the intermixing of constituent elements and to the formation and evolution of voids.

SUPPLEMENTARY MATERIAL

See supplementary material for (1) ion fluence dependent variation in the lattice constant; (2) Table S1: Structural parameters obtained from GXRD; (3) XANES spectra recorded near the Zn-K edge before and after Ar^{+}-ion irradiation; and (4) snapshot of depth dependent Ar^{+}-ion distribution with full damage cascade, obtained by SRIM simulation.

ACKNOWLEDGMENTS

[1]S. Facsko, T. Dekorsy, C. Koerdt, C. Trappe, H. Kurz, A. Vogt, and H. L. Hartnagel, Science **285**, 1551 (1999).

[2]O. Rodríguez de la Fuente, M. A. González-Barrio, V. Navarro, B. M. Pabón, I. Palacio, and A. Mascaraque, J. Phys. Condens. Matter **25**, 484008 (2013).

[3]P. Sioshansi, Thin Solid Films **118**, 61 (1984).

[4]J. R. Conrad, J. L. Radtke, R. A. Dodd, F. J. Worzala, and N. C. Tran, J. Appl. Phys. **62**, 4591 (1987).

[5]T. Choudhury, S. O. Saied, J. L. Sullivan, and A. M. Abbot, J. Phys. D Appl. Phys. **22**, 1185 (1989).

[6]H. Kazuhito, I. Hiroshi, and F. Akira, Jpn. J. Appl. Phys. **44**, 8269 (2005).

[7]A. V. Singh, R. M. Mehra, A. Yoshida, and A. Wakahara, J. Appl. Phys. **95**, 3640 (2004).

[8]S. Na-Phattalung, M. F. Smith, K. Kim, M.-H. Du, S.-H. Wei, S. B. Zhang, and S. Limpijumnong, Phys. Rev. B **73**, 125205 (2006).

[9]M.-T. Tsai, Z.-P. Yang, T.-S. Jing, H.-H. Hsieh, Y.-C. Yao, T.-Y. Lin, Y.-F. Chen, and Y.-J. Lee, Sol. Energy Mater. Sol. Cells **136**, 17 (2015).

[10]N. Matsunami, O. Fukuoka, M. Tazawa, and M. Sataka, Surf. Coat. Technol. **196**, 50 (2005).

[11]D. C. Agarwal, R. S. Chauhan, D. K. Avasthi, S. A. Khan, D. Kabiraj, and I. Sulania, J. Appl. Phys. **104**, 024304 (2008).

[12]A. Barman, C. P. Saini, P. Sarkar, B. Satpati, S. R. Bhattacharyya, D. Kabiraj, D. Kanjilal, S. Dhar, and A. Kanjilal, J. Appl. Phys. **118**, 224903 (2015).

[13]A. Barman, C. P. Saini, P. K. Sarkar, A. Roy, B. Satpati, D. Kanjilal, S. K. Ghosh, S. Dhar, and A. Kanjilal, Appl. Phys. Lett. **108**, 244104 (2016).

[14]C. P. Saini, A. Barman, B. Satpati, S. R. Bhattacharyya, D. Kanjilal, and A. Kanjilal, Appl. Phys. Lett. **108**, 011907 (2016).

[15]C. P. Saini, A. Barman, D. Das, B. Satpati, S. R. Bhattacharyya, D. Kanjilal, A. Ponomaryov, S. Zvyagin, and A. Kanjilal, J. Phys. Chem. C **121**, 278 (2017).

[16]B. M. Pabón, J. I. Beltrán, G. Sánchez-Santolino, I. Palacio, J. López-Sánchez, J. Rubio-Zuazo, J. M. Rojo, P. Ferrer, A. Mascaraque, M. C. Muñoz, M. Varela, G. R. Castro, and O. Rodríguez de la Fuente, Nat. Commun. **6**, 6147 (2015).

[17]X. W. Zhang, C. C. Liu, and G. R. Han, paper presented at the Materials Science Forum (2009), see https://doi.org/10.4028/www.scientific.net/MSF.620-622.707.

[18]Y. Mi, L. Wen, R. Xu, Z. Wang, D. Cao, Y. Fang, and Y. Lei, Adv. Energy Mater. **6**, 1501496 (2015).

[19]G. A. Kumar, M. V. R. Reddy, and R. K. Narasimha, IOP Confer. Series Mater. Sci. Eng. **73**, 012133 (2015).

[20]I. Ozen and M. A. Gulgun, Advan. Sci. Technol. **45**, 1316 (2006).

[21]M. Kumar, A. Kanjilal, and T. Som, AIP Adv. **3**, 092126 (2013).

[22]B. C. Mohanty, Y. H. Jo, D. H. Yeon, I. J. Choi, and Y. S. Cho, Appl. Phys. Lett. **95**, 062103 (2009).

[23]S. Stepanov, 3rd Autumn School on X-ray Scattering from Surfaces and Thin Layers, Smolenice, Slovakia, 1–4 October 1997.

[24]E. S. Andrés, M. Toledano-Luque, A. del Prado, M. A. Navacerrada, I. Mártil, G. González-Díaz, W. Bohne, J. Röhrich, and E. Strub, J. Vac. Sci. Technol. **23**, 1523 (2005).

[25]K. Sang-Woo, F. Shizuo, and F. Shigeo, Jpn. J. Appl. Phys. **41**, L543 (2002).

[26]S. H. Park, T. Hanada, D. C. Oh, T. Minegishi, H. Goto, G. Fujimoto, J. S. Park, I. H. Im, J. H. Chang, M. W. Cho, T. Yao, and K. Inaba, Appl. Phys. Lett. **91**, 231904 (2007).

[27]N. R. Mathews, E. R. Morales, M. A. Cortés-Jacome, and J. A. Toledo Antonio, Solar Energy **83**, 1499 (2009).

[28]H. Kazumasa, D. Theeradetch, and A. Isamu, Jpn. J. Appl. Phys. **32**, 1528 (1993).

[29]N. Itoh, J. C. Rhee, T. Kawabata, and S. Koike, J. Appl. Phys. **58**, 1828 (1985).

[30]P. Farzinpour, A. Sundar, K. D. Gilroy, Z. E. Eskin, R. A. Hughes, and S. Neretina, Nanotechnology **23**, 495604 (2012).

[31]K. Watanabe, D.-H. Lee, I. Sakaguchi, K. Nomura, T. Kamiya, H. Haneda, H. Hosono, and N. Ohashi, Appl. Phys. Lett. **103**, 201904 (2013).

[32]S. Shirasaki, H. Yamamura, H. Haneda, K. Kakegawa, and J. Moori, J. Chem. Phys. **73**, 4640 (1980).

[33]G. Knöner, K. Reimann, R. Röwer, U. Södervall, and H.-E. Schaefer, Proc. Natl. Acad. Sci. U.S.A. **100**, 3870 (2003).

[34]P. K. Giri, S. Kumari, and D. K. Goswami, Appl. Surf. Sci. **256**, 384 (2009).

[35]I. P. Jain and G. Agarwal, Surf. Sci. Rep. **66**, 77 (2011).

[36]P. K. Haff and Z. E. Switkowski, J. Appl. Phys. **48**, 3383 (1977).